Acta Cryst E CRYSTALLOGRAPHIC COMMUNICATIONS

ISSN 2056-9890

Crystal structure, Hirshfeld surface analysis and interaction energy and DFT studies of 1-methyl-3-(prop-2-yn-1-yl)-2,3-dihydro-1*H*-1,3-benzodiazol-2-one

Asmaa Saber,[a] Mohamed Srhir,[a]* Tuncer Hökelek,[b] Joel T. Mague,[c] Noureddine Hamou Ahabchane,[a] Nada Kheira Sebbar[d,a] and El Mokhtar Essassi[a]

[a]Laboratoire de Chimie Organique Hétérocyclique URAC 21, Pôle de Compétence Pharmacochimie, Av. Ibn Battouta, BP 1014, Faculté des Sciences, Université Mohammed V, Rabat, Morocco, [b]Department of Physics, Hacettepe University, 06800 Beytepe, Ankara, Turkey, [c]Department of Chemistry, Tulane University, New Orleans, LA 70118, USA, and [d]Laboratoire de Chimie Appliquée et Environnement, Equipe de Chimie Bioorganique Appliquée, Faculté des Sciences, Université Ibn Zohr, Agadir, Morocco. *Correspondence e-mail: mohamedsrhir2018@gmail.com

Received 12 November 2019
Accepted 21 November 2019

Edited by A. J. Lough, University of Toronto, Canada

Keywords: crystal structure; benzimidazol-2-one; hydrogen bond; C—H···π(ring) interaction; π-stacking; Hirshfeld surface.

CCDC reference: 1967468

Supporting information: this article has supporting information at journals.iucr.org/e

In the title molecule, $C_{11}H_{10}N_2O$, the dihydrobenzimidazol-2-one moiety is essentially planar, with the prop-2-yn-1-yl substituent rotated well out of this plane. In the crystal, $C-H_{Mthy}\cdots\pi$(ring) interactions and $C-H_{Prop}\cdots O_{Dhyr}$ (Mthy = methyl, Prop = prop-2-yn-1-yl and Dhyr = dihydro) hydrogen bonds form corrugated layers parallel to $(10\bar{1})$, which are associated through additional $C-H_{Bnz}\cdots O_{Dhyr}$ (Bnz = benzene) hydrogen bonds and head-to-tail, slipped, π-stacking [centroid-to-centroid distance = 3.7712 (7) Å] interactions between dihydrobenzimidazol-2-one moieties. The Hirshfeld surface analysis of the crystal structure indicates that the most important contributions to the crystal packing are from H···H (44.1%), H···C/C···H (33.5%) and O···H/H···O (13.4%) interactions. Hydrogen-bonding and van der Waals interactions are the dominant interactions in the crystal packing. Computational chemistry calculations indicate that in the crystal, C—H···O hydrogen-bond energies are 46.8 and 32.5 (for $C-H_{Prop}\cdots O_{Dhyr}$) and 20.2 (for $C-H_{Bnz}\cdots O_{Dhyr}$) kJ mol^{-1}. Density functional theory (DFT) optimized structures at the B3LYP/6–311 G(d,p) level are compared with the experimentally determined molecular structure in the solid state. The HOMO–LUMO behaviour was elucidated to determine the energy gap.

1. Chemical context

Benzimidazole is an aromatic heterocyclic organic compound that plays an important role in medicinal chemistry and pharmacology. The most prominent benzimidazole moiety present in nature is *N*-ribosyl-dimethylbenzimidazole and it serves as the axial ligand for cobalt in vitamin B12 (Walia *et al.*, 2011). Benzimidazole derivatives possess many biological activities such as anti-microbial, anti-fungal, anti-histaminic, anti-inflammatory, anti-viral, anti-oxidant, anti-cancer and anti-ulcerative (Farukh & Mubashira, 2009; Ayhan-Kılcıgil *et al.*, 2007; Soderlind *et al.*, 1999; Luo *et al.*, 2011; Navarrete-Vázquez *et al.*, 2011). They are considered to be an important moiety for the development of molecules of pharmaceutical interest (Mondieig *et al.*, 2013; Lakhrissi *et al.*, 2008). As a continuation of our research on the development of N-substituted benzimidazole derivatives and the evaluation of their potential pharmacological activities (Saber *et al.*, 2018*a*,*b*, 2020; Ouzidan *et al.*, 2011), we have studied the

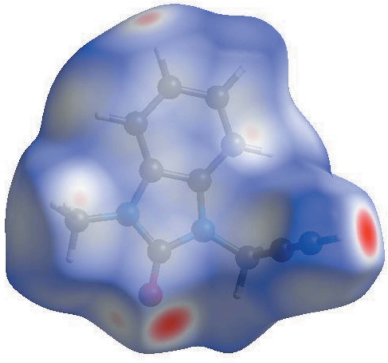

alkylation reaction of iodomethane with 1-(prop-2-ynyl)-1*H*-benzoimidazol-2(3*H*)-one in the presence of tetra-*n*-butylammonium bromide as catalyst and potassium carbonate as base, to give the title compound, **I** in good yield. We report herein on its synthesis, the molecular and crystal structures along with the Hirshfeld surface analysis and the intermolecular interaction energies and the density functional theory (DFT) computational calculations carried out at the B3LYP/6–311 G(d,p) level for comparison with the experimentally determined molecular structure in the solid state.

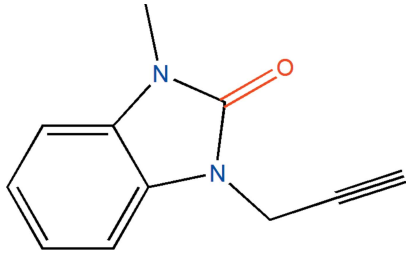

2. Structural commentary

In the title compound, the dihydrobenzimidazol-2-one moiety is planar to within 0.0160 (8) Å (r.m.s. deviation = 0.0082) with atom C7 deviating the most from the mean plane and a prop-2-yn-1-yl substituent rotated well out of this plane as shown by the C1—N2—C9—C10 torsion angle of 62.16 (13)° (Fig. 1).

3. Supramolecular features

In the crystal, inversion dimers are formed by pairs of C—$H_{Mthy}\cdots Cg1^{i}$ interactions [Mthy = methyl; symmetry code: (i) $-x, 1-y, 1-z$; *Cg*1 is the centroid of the benzene (*A*; C1–C6), ring]; which are connected along the *b*-axis direction by C—$H_{Bnz}\cdots O_{Dhyr}$ hydrogen bonds (Bnz = benzene and Dhyr = dihydro) and along the *a*-axis direction at *ca* 90° to this and parallel to $(10\bar{1})$ by inversion-related C—$H_{Prop}\cdots O_{Dhyr}$ hydrogen bonds (Table 1). The resulting corrugated layers are parallel to $(10\bar{1})$ and are connected in pairs by slipped, head-to-tail π-stacking interactions between the dihydrobenzimidazol-2-one moieties, [$Cg2\cdots Cg1^{ii}$ = 3.7712 (7) Å, dihedral angle = 0.96 (6)°; symmetry code: (ii) $1-x, 1-y, 1-z$; *Cg*1 and *Cg*2 are the centroids of rings *A* and *B* (N1/N2/C1/C6/C7) and C—$H_{Prop}\cdots O_{Dhyr}$ (Prop = prop-2-yn-1-yl) hydrogen bonds (Table 1, Figs. 2 and 3).

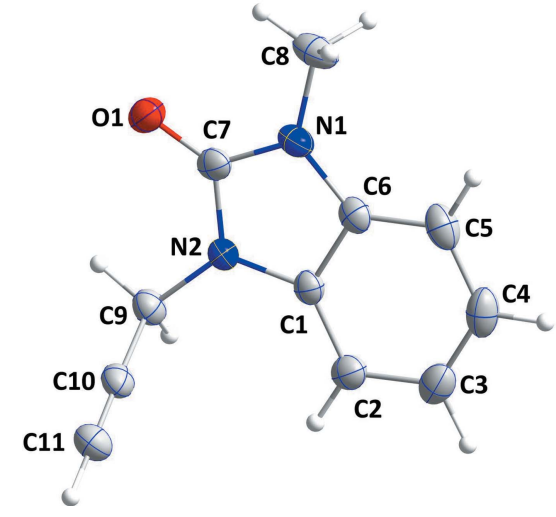

Figure 1
The molecular structure of the title compound with the atom-numbering scheme. Displacement ellipsoids are drawn at the 50% probability level.

Table 1
Hydrogen-bond geometry (Å, °).

*Cg*1 is the centroid of the C1–C6 benzene ring.

D—H···*A*	*D*—H	H···*A*	*D*···*A*	*D*—H···*A*
C3—H3···O1^{ix}	1.005 (15)	2.566 (15)	3.4885 (15)	152.6 (11)
C8—H8*C*···*Cg*1^{v}	1.004 (16)	2.626 (15)	3.5413 (13)	151.1 (12)
C9—H9*B*···O1^{vi}	0.978 (15)	2.347 (15)	3.3198 (14)	172.9 (12)
C11—H11···O1^{vii}	1.010 (15)	2.181 (15)	3.1569 (15)	162.1 (12)

Symmetry codes: (v) $-x, -y+1, -z+1$; (vi) $-x+\frac{1}{2}, y-\frac{1}{2}, -z+\frac{3}{2}$; (vii) $-x+\frac{3}{2}, y-\frac{1}{2}, -z+\frac{3}{2}$; (ix) $x, y-1, z$.

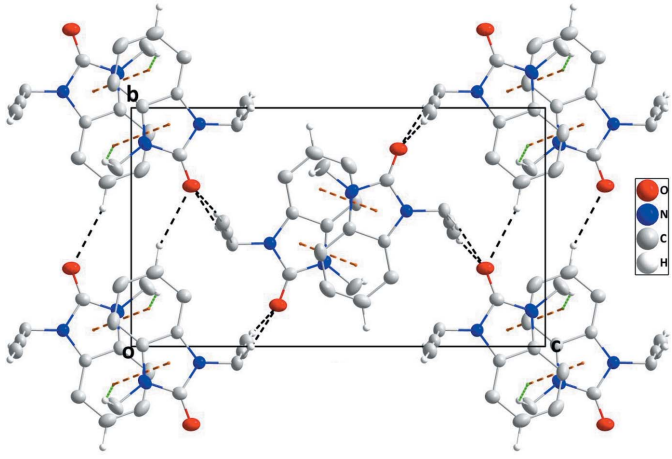

Figure 2
A partial packing diagram viewed along the *a*-axis direction with C—H···O hydrogen bonds, C—H···π(ring) and π-stacking interactions shown, respectively, by black, green and orange dashed lines.

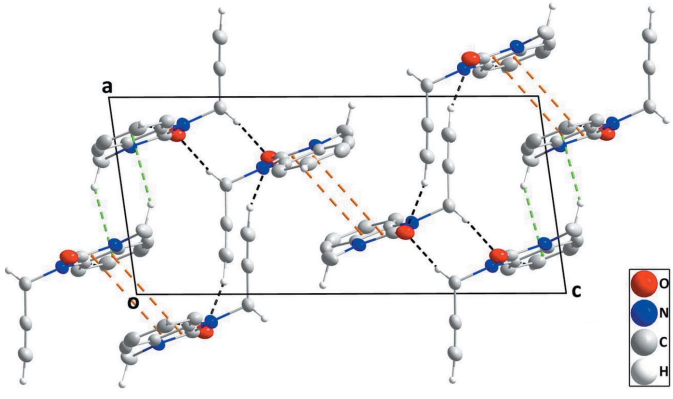

Figure 3
A partial packing diagram viewed along the *b*-axis direction with intermolecular interactions depicted as in Fig. 2.

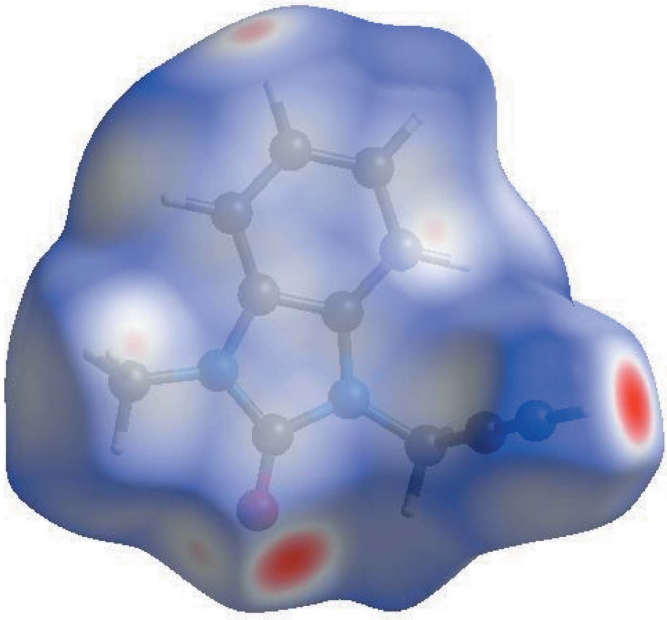

Figure 4
View of the three-dimensional Hirshfeld surface of the title compound plotted over d_{norm} in the range −0.3997 to 1.3219 a.u.

4. Hirshfeld surface analysis

In order to visualize the intermolecular interactions in the crystal of the title compound, a Hirshfeld surface (HS) analysis (Hirshfeld, 1977; Spackman & Jayatilaka, 2009) was carried out using *Crystal Explorer 17.5* (Turner *et al.*, 2017). In the HS plotted over d_{norm} (Fig. 4), the white surface indicates contacts with distances equal to the sum of van der Waals radii, and the red and blue colours indicate distances shorter (in close contact) or longer (distant contact) than the van der Waals radii, respectively (Venkatesan *et al.*, 2016). The bright-red spots appearing near O1 and the hydrogen atom H11 indicate their roles as the donors and/or acceptors, respectively; they also appear as blue and red regions corresponding to positive and negative potentials on the HS mapped over electrostatic potential (Spackman *et al.*, 2008; Jayatilaka *et al.*, 2005) as shown in Fig. 5. The blue regions indicate positive electrostatic potential (hydrogen-bond donors), while the red regions indicate negative electrostatic potential (hydrogen-bond acceptors). The shape-index of the HS is a tool to visualize
π–π stacking by the presence of adjacent red and blue triangles; if there are no adjacent red and/or blue triangles, then there are no π–π interactions. Fig. 6 clearly suggests that there are π– π interactions in (I).

Table 2
Selected interatomic distances (Å).

O1···H9*A*	2.491 (14)	C11···O1^{vii}	3.1569 (15)
O1···H3^{i}	2.566 (15)	C2···H8*A*^{iv}	2.82 (2)
O1···H8*B*	2.516 (19)	C3···H8*C*^{v}	2.859 (15)
O1···H9*B*^{ii}	2.346 (14)	C3···H8*A*^{iv}	2.92 (2)
O1···H11^{iii}	2.181 (15)	C4···H8*C*^{v}	2.810 (15)
C2···C10	3.3889 (16)	C5···H8*C*^{v}	2.935 (15)
C3···C8^{iv}	3.5335 (17)	C8···H5	2.983 (14)
C4···C8^{v}	3.4947 (17)	C9···H2	2.975 (14)
C4···C7^{iv}	3.5437 (16)	C10···H4^{viii}	2.976 (15)
C5···C8^{v}	3.5884 (17)	C11···H5^{iv}	2.865 (15)
C6···C6^{iv}	3.5349 (14)	C11···H4^{viii}	2.705 (15)
C9···O1^{vi}	3.3198 (14)		

Symmetry codes: (i) $x, y+1, z$; (ii) $-x+\frac{1}{2}, y+\frac{1}{2}, -z+\frac{3}{2}$; (iii) $-x+\frac{3}{2}, y+\frac{1}{2}, -z+\frac{3}{2}$; (iv) $-x+1, -y+1, -z+1$; (v) $-x, -y+1, -z+1$; (vi) $-x+\frac{1}{2}, y-\frac{1}{2}, -z+\frac{3}{2}$; (vii) $-x+\frac{3}{2}, y-\frac{1}{2}, -z+\frac{3}{2}$; (viii) $x+\frac{1}{2}, -y+\frac{1}{2}, z+\frac{1}{2}$.

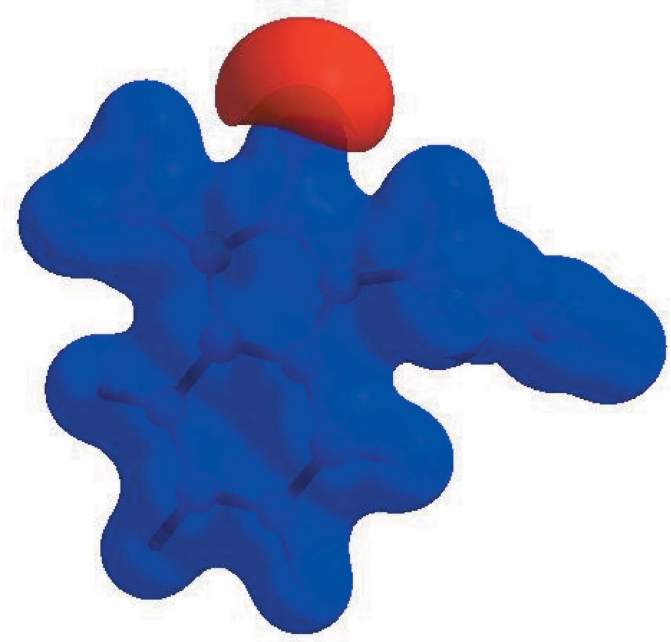

Figure 5
View of the three-dimensional Hirshfeld surface of the title compound plotted over electrostatic potential energy in the range −0.0500 to 0.0500 a.u. using the STO-3 G basis set at the Hartree–Fock level of theory. Hydrogen-bond donors and acceptors are shown as blue and red regions around the atoms corresponding to positive and negative potentials, respectively.

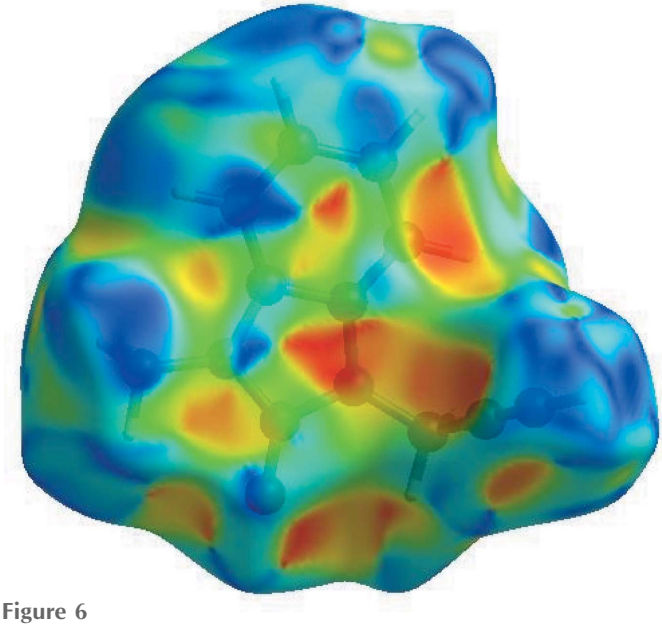

Figure 6
Hirshfeld surface of the title compound plotted over shape-index.

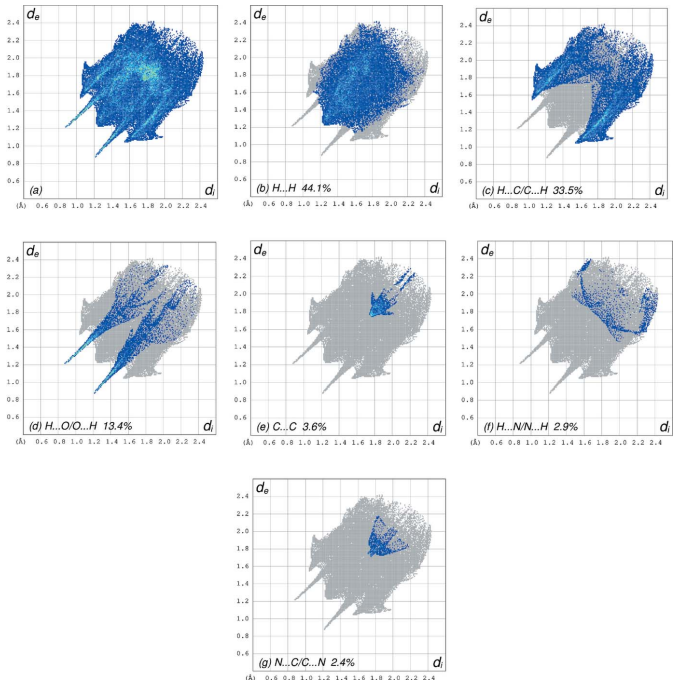

Figure 7
The full two-dimensional fingerprint plots for the title compound, showing (*a*) all interactions, and delineated into (*b*) H···H, (*c*) H···C/C···H, (*d*) H···O/O···H, (*e*) C···C, (*f*) H···N/N···H and (*g*) N···C/C···N interactions. The d_i and d_e values are the closest internal and external distances (in Å) from given points on the Hirshfeld surface contacts.

The overall two-dimensional fingerprint plot, Fig. 7*a*, and those delineated into H···H, H···C/C···H, H···O/O ··· H, C···C, H···N/N···H and N···C/C···N contacts (McKinnon *et al.*, 2007) are illustrated in Fig. 7*b–g*, respectively, together with their relative contributions to the Hirshfeld surface. The most important interaction is H···H contributing 44.1% to the overall crystal packing, which is reflected in Fig. 7*b* as widely scattered points of high density due to the large hydrogen content of the molecule with the tip at $d_e = d_i = 1.22$ Å. The presence of C—H···π interactions gives rise to pairs of characteristic wings in the fingerprint plot delineated into H···C/C···H contacts, Fig. 7*c*., contributing 33.5% to the HS (Table 2); these are viewed as pairs of spikes with the tips at $d_e + d_i = 2.56$ Å. The pair of wings in Fig. 7*d* has a symmetrical distribution of points with the edges at $d_e + d_i = 2.09$ Å arising from the H···O/O···H contacts (13.4% contribution). The C···C contacts, Fig. 7*e*, have an arrow-shaped distribution of points with the tip at $d_e = d_i = 1.75$ Å. The H···N/N···N contacts, contributing 2.9% to the overall crystal packing, are depicted in Fig. 7*f* as widely scattered points. Finally, the N···C/C···N interactions, contributing 2.4% to the overall crystal packing, are shown in Fig. 7*g* as tiny characteristic wings with the tips at $d_e + d_i = 3.45$ Å.

The Hirshfeld surface representations with the function d_{norm} plotted onto the surface are shown for the H···H, H···C/C···H and H···O/O···H interactions in Fig. 8*a–c*, respectively.

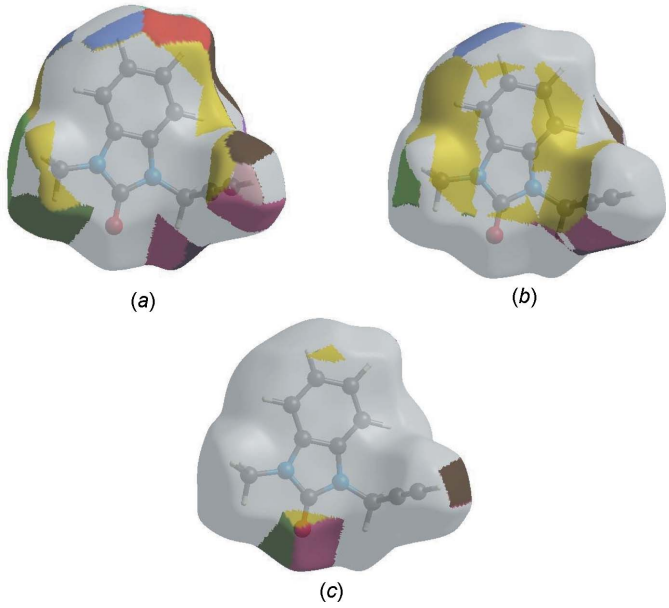

Figure 8
The Hirshfeld surface representations with the function d_{norm} plotted onto the surface for (*a*) H···H, (*b*) H···C/C···H and (*c*) H···O/O···H interactions.

The Hirshfeld surface analysis confirms the importance of H-atom contacts in establishing the packing. The large number of H···H, H···C/C···H and H··· O/O···H interactions suggest that van der Waals interactions and hydrogen bonding play the major roles in the crystal packing (Hathwar *et al.*, 2015).

5. Interaction energy calculations

The intermolecular interaction energies were calculated using the CE–B3LYP/6–31G(d,p) energy model available in *CrystalExplorer17.5* (Turner *et al.*, 2017), where a cluster of molecules is generated by applying crystallographic symmetry operations with respect to a selected central molecule within the default radius of 3.8 Å (Turner *et al.*, 2014). The total intermolecular energy (E_{tot}) is the sum of electrostatic (E_{ele}), polarization (E_{pol}), dispersion (E_{dis}) and exchange-repulsion (E_{rep}) energies (Turner *et al.*, 2015) with scale factors of 1.057, 0.740, 0.871 and 0.618, respectively (Mackenzie *et al.*, 2017). Hydrogen-bonding interaction energies (in kJ mol^{-1}) were calculated to be −17.4 (E_{ele}), −3.5 (E_{pol}), −62.6 (E_{dis}), 46.5 (E_{rep}) and −46.8 (E_{tot}) for C11—H11···O1, −12.4 (E_{ele}), −1.9 (E_{pol}), −41.6 (E_{dis}), 29.6 (E_{rep}) and −32.5 (E_{tot}) for C9—H9*B*···O1 and −13.7 (E_{ele}), −3.7 (E_{pol}), −15.5 (E_{dis}), 17.0 (E_{rep}) and −20.2 (E_{tot}) for C3—H3···O1.

6. DFT calculations

The optimized structure of the title compound in the gas phase was generated theoretically *via* density functional theory (DFT) using the standard B3LYP functional and 6–311 G(d,p) basis-set calculations (Becke, 1993) as implemented in *GAUSSIAN 09* (Frisch *et al.*, 2009). The theoretical and

Table 3
Comparison of the selected (X-ray and DFT) geometric data (Å, °).

Bonds/angles	X-ray	B3LYP/6–311 G(d,p)
O1—C7	1.2281 (13)	1.24660
N1—C7	1.3735 (14)	1.39764
N1—C6	1.3874 (15)	1.40100
N1—C8	1.4526 (14)	1.45375
N2—C7	1.3807 (14)	1.40268
N2—C1	1.3910 (13)	1.40222
N2—C9	1.4545 (14)	1.46036
C7—N1—C6	110.19 (9)	110.10303
C7—N1—C8	124.14 (10)	122.94288
C6—N1—C8	125.66 (10)	126.95366
C7—N2—C1	110.16 (9)	110.18664
C7—N2—C9	123.55 (9)	122.02491
C1—N2—C9	126.00 (9)	126.78733
C2—C1—N2	131.64 (10)	132.00719

experimental results are in good agreement (Table 3). The highest-occupied molecular orbital (HOMO), acting as an electron donor, and the lowest-unoccupied molecular orbital (LUMO), acting as an electron acceptor, are very important parameters for quantum chemistry. When the energy gap is small, the molecule is highly polarizable and has high chemical reactivity. The DFT calculations provide some important information on the reactivity and site selectivity of the molecular framework. E_{HOMO} and E_{LUMO} clarify the inevitable charge-exchange collaboration inside the studied material and are given in Table 4 along with the electronegativity (χ), hardness (η), potential (μ), electrophilicity (ω) and softness (σ). The significance of η and σ is for the evaluation of both the reactivity and stability. The electron transition from the HOMO to the LUMO energy level is shown in Fig. 9. The

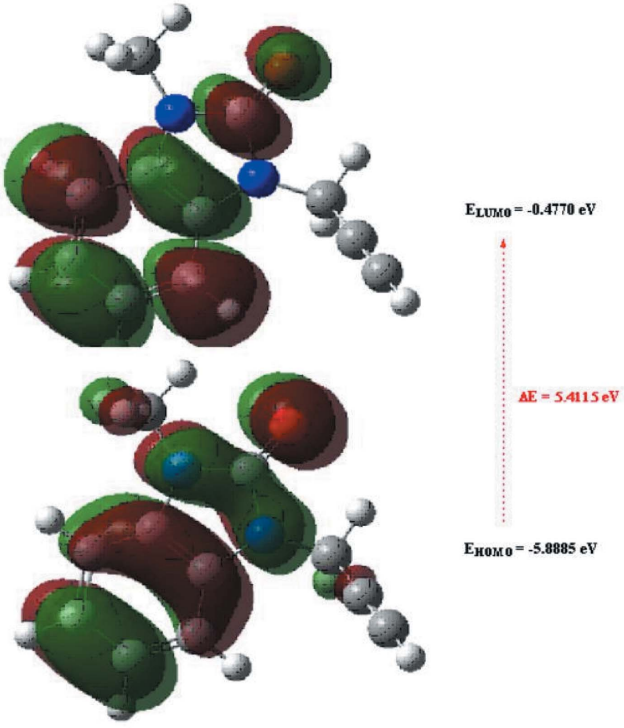

Figure 9
The energy band gap of the title compound.

Table 4
Calculated energies for the title compound.

Molecular Energy (a.u.) (eV)	
Total Energy *TE* (eV)	−16594.1662
E_{HOMO} (eV)	−5.8885
E_{LUMO} (eV)	−0.4770
Energy gap, ΔE (eV)	5.4115
Dipole moment, μ (Debye)	2.8313
Ionization potential, I (eV)	5.8885
Electron affinity, A	2.6040
Electro negativity, χ	0.31828
Hardness, η	2.7058
Electrophilicity index, ω	1.8719
Softness, σ	0.3696
Fraction of electron transferred, ΔN	0.7054

HOMO and LUMO are localized in the plane extending from the whole 1-methyl-3-(prop-2-yn-1-yl)-2,3-dihydro-1*H*-1,3-benzodiazol-2-one ring. The energy band gap [$\Delta E = E_{LUMO} - E_{HOMO}$] of the molecule is about 5.4115 eV, and the frontier molecular orbital energies, E_{HOMO} and E_{LUMO} are −5.8885 and −0.4770 eV, respectively.

7. Database survey

The syntheses of several N-substituted benzimidazol-2-one analogues have been reported (Saber *et al.*, 2018*a*,*b*; 2020; Belaziz *et al.*, 2012; Bouayad *et al.*, 2015; Belaziz *et al.*, 2013). In a search of the Cambridge Crystallographic Database (CSD; Version 5.40, update of September 2019; Groom *et al.*, 2016) using benzimidazol-2-one with an exocyclic carbon atom bound to each nitrogen generated 94 hits. In these, the bicyclic ring system is either planar, has a slight twist end-to-end, or, in the cases where the exocyclic substituents form a ring, has a very shallow bowl shape.

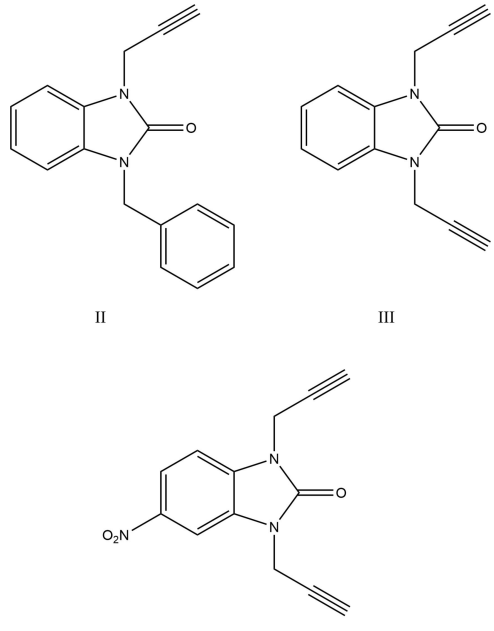

The closest examples to the title compound, **I**, are **II** (HISFUN; Saber *et al.*, 2018*b*), **III** (URAQAG; Ouzidan *et al.*,

2011*a*) and **IV** (AGAXOX; Kandri Rodi *et al.*, 2013). In the title compound, the C—N bonds to the exocyclic groups are 1.4526 (14) and 1.4545 (19) Å while in **II**–**IV** the corresponding distances range from 1.445 (3) to 1.4632 (11) Å, and so are quite comparable. The exocyclic groups in **I** are in an *anti*-arrangement with the prop-2-yn-1-yl group rotated by 62.16 (13)° out of the plane of the bicyclic moiety (as measured by the C1—N2—C9—C10 torsion angle). In the other three, these substituents are also *anti* and in **II** the corresponding torsion angle is 73.46 (18)° while in **III** they are 82.58 (15) and 74.31 (14)°. In **IV** the torsion angles are 106.0 (3) and 113.4 (3)° indicating a rotation in the opposite direction from the first three.

8. Synthesis and crystallization

To a mixture of 1-(prop-2-ynyl)-1*H*-benzimidazol-2(3*H*)-one (3.61 mmol), iodomethane (6.73 mmol) and potassium carbonate (6.24 mmol) in DMF (15 ml) was added a catalytic amount of tetra-*n*-butylammonium bromide (0.37 mmol). The mixture was stirred for 24 h. The solid material was removed by filtration and the solvent evaporated under vacuum. The solid product was purified by recrystallization from ethanol to afford colorless crystals (yield: in 82%).

9. Refinement

Crystal data, data collection and structure refinement details are summarized in Table 5. Hydrogen atoms were located in a difference Fourier map and refined freely.

Table 5
Experimental details.

Crystal data	
Chemical formula	$C_{11}H_{10}N_2O$
M_r	186.21
Crystal system, space group	Monoclinic, $P2_1/n$
Temperature (K)	150
a, b, c (Å)	7.1507 (3), 8.8177 (4), 15.4602 (7)
β (°)	97.914 (2)
V (Å^3)	965.52 (7)
Z	4
Radiation type	Cu $K\alpha$
μ (mm^{-1})	0.68
Crystal size (mm)	0.32 × 0.31 × 0.12
Data collection	
Diffractometer	Bruker D8 VENTURE PHOTON 100 CMOS
Absorption correction	Multi-scan (*SADABS*; Krause *et al.*, 2015)
T_{min}, T_{max}	0.83, 0.92
No. of measured, independent and observed [$I > 2\sigma(I)$] reflections	6896, 1812, 1679
R_{int}	0.030
(sin $\theta/\lambda)_{max}$ (Å^{-1})	0.610
Refinement	
$R[F^2 > 2\sigma(F^2)]$, $wR(F^2)$, S	0.033, 0.086, 1.06
No. of reflections	1812
No. of parameters	168
H-atom treatment	All H-atom parameters refined
$\Delta\rho_{max}$, $\Delta\rho_{min}$ (e Å^{-3})	0.18, −0.19

Computer programs: *APEX3* and *SAINT* (Bruker, 2016), *SHELXT* (Sheldrick, 2015*a*), *SHELXL2018* (Sheldrick, 2015*b*), *DIAMOND* (Brandenburg & Putz, 2012) and *SHELXTL* (Sheldrick, 2008).

Funding information

The support of NSF–MRI grant No. 1228232 for the purchase of the diffractometer and Tulane University for support of the Tulane Crystallography Laboratory are gratefully acknowledged. TH is grateful to Hacettepe University Scientific Research Project Unit (grant No. 013 D04 602 004).

References

Ayhan-Kılcıgil, G., Kus, G., Özdamar, E. D., Can-Eke, B. & Iscan, M. (2007). *Arch. Pharm. Chem. Life Sci.* **340**, 607–611.
Becke, A. D. (1993). *J. Chem. Phys.* **98**, 5648–5652.
Belaziz, D., Kandri Rodi, Y., Essassi, E. M. & El Ammari, L. (2012). *Acta Cryst.* E**68**, o1276.
Belaziz, D., Kandri Rodi, Y., Ouazzani Chahdi, F., Essassi, E. M., Saadi, M. & El Ammari, L. (2013). *Acta Cryst.* E**69**, o122.
Bouayad, K., Kandri Rodi, Y., Ouzidan, Y., Essassi, E. M., Saadi, M. & El Ammari, L. (2015). *Acta Cryst.* E**71**, o735–o736.
Brandenburg, K. & Putz, H. (2012). *DIAMOND*. Crystal Impact GbR, Bonn, Germany.
Bruker (2016). *APEX3*, *SAINT* and *SADABS*. Bruker AXS, Inc., Madison, Wisconsin, USA.
Farukh, A. & Mubashira, A. (2009). *Eur. J. Med. Chem.* **44**, 834–844.
Frisch, M. J., *et al.* (2009). *GAUSSIAN09*. Gaussian Inc., Wallingford, CT, US
Groom, C. R., Bruno, I. J., Lightfoot, M. P. & Ward, S. C. (2016). *Acta Cryst.* B**72**, 171–179.
Hathwar, V. R., Sist, M., Jørgensen, M. R. V., Mamakhel, A. H., Wang, X., Hoffmann, C. M., Sugimoto, K., Overgaard, J. & Iversen, B. B. (2015). *IUCrJ*, **2**, 563–574.
Hirshfeld, H. L. (1977). *Theor. Chim. Acta*, **44**, 129–138.
Jayatilaka, D., Grimwood, D. J., Lee, A., Lemay, A., Russel, A. J., Taylor, C., Wolff, S. K., Cassam-Chenai, P. & Whitton, A. (2005). *TONTO – A System for Computational Chemistry.* Available at: http://hirshfeldsurface.net/
Kandri Rodi, Y., Misbahi, K., El-Ghayoury, A., Zorina, L., Essassi, E. M. & El Ammari, L. (2013). *Acta Cryst.* E**69**, o1159.
Krause, L., Herbst-Irmer, R., Sheldrick, G. M. & Stalke, D. (2015). *J. Appl. Cryst.* **48**, 3–10.
Lakhrissi, B., Benksim, A., Massoui, M., Essassi, E. M., Lequart, V., Joly, N., Beaupère, D., Wadouachi, A. & Martin, P. (2008). *Carbohydr. Res.* **343**, 421–433.
Luo, Y., Yao, J. P., Yang, L., Feng, C. L., Tang, W., Wang, G. F., Zuo, J. P. & Lu, W. (2011). *Arch. Pharm. Pharm. Med. Chem.* **344**, 78–83.
Mackenzie, C. F., Spackman, P. R., Jayatilaka, D. & Spackman, M. A. (2017). *IUCrJ*, **4**, 575–587.
McKinnon, J. J., Jayatilaka, D. & Spackman, M. A. (2007). *Chem. Commun.* pp. 3814–3816.
Mondieig, D., Lakhrissi, L., El Assyry, A., Lakhrissi, B., Negrier, P., Essassi, E. M., Massoui, M., Michel Leger, J. & Benali, B. (2013). *J. Mar. Chim. Heterocycl.* **12**, 51–61.
Navarrete-Vázquez, G., Cedillo, R., Hernández-Campos, A., Yépez, L., Hernández-Luis, F., Valdez, J., Morales, R., Cortés, R., Hernández, M. & Castillo, R. (2011). *Bioorg. Med. Chem.* **11**, 187–190.
Ouzidan, Y., Kandri Rodi, Y., Fronczek, F. R., Venkatraman, R., El Ammari, L. & Essassi, E. M. (2011). *Acta Cryst.* E**67**, o362–o363.
Ouzidan, Y., Kandri Rodi, Y., Jasinski, J. P., Butcher, R. J., Golen, J. A. & El Ammari, L. (2011*a*). *Acta Cryst.* E**67**, o1091.

Saber, A., Sebbar, N. K., Hökelek, T., El hafi, M., Mague, J. T. & Essassi, E. M. (2018*b*). *Acta Cryst.* E**74**, 1842–1846.
Saber, A., Sebbar, N. K., Hökelek, T., Hni, B., Mague, J. T. & Essassi, E. M. (2018*a*). *Acta Cryst.* E**74**, 1746–1750.
Saber, A., Sebbar, N. K., Sert, Y., Alzaqri, N., Hökelek, T., El Ghayati, L., Talbaoui, A., Mague, J. T., Filali Baba, Y., Urrutigoîty, M. & Essassi, E. M. (2020). *J. Mol. Struct.* **1200**, 127174.
Sheldrick, G. M. (2008). *Acta Cryst.* A**64**, 112–122.
Sheldrick, G. M. (2015*a*). *Acta Cryst.* A**71**, 3–8.
Sheldrick, G. M. (2015*b*). *Acta Cryst.* C**71**, 3–8.
Soderlind, K. J., Gorodetsky, B., Singh, A. K., Bachur, N., Miller, G. G. & Lown, J. W. (1999). *Anticancer Drug. Des.* **14**, 19–36.
Spackman, M. A. & Jayatilaka, D. (2009). *CrystEngComm*, **11**, 19–32.
Spackman, M. A., McKinnon, J. J. & Jayatilaka, D. (2008). *CrystEngComm*, **10**, 377–388.
Turner, M. J., Grabowsky, S., Jayatilaka, D. & Spackman, M. A. (2014). *J. Phys. Chem. Lett.* **5**, 4249–4255.
Turner, M. J., McKinnon, J. J., Wolff, S. K., Grimwood, D. J., Spackman, P. R., Jayatilaka, D. & Spackman, M. A. (2017). *CrystalExplorer17*. The University of Western Australia.
Turner, M. J., Thomas, S. P., Shi, M. W., Jayatilaka, D. & Spackman, M. A. (2015). *Chem. Commun.* **51**, 3735–3738.
Venkatesan, P., Thamotharan, S., Ilangovan, A., Liang, H. & Sundius, T. (2016). *Spectrochim. Acta Part A*, **153**, 625–636.
Walia, R., Hedaitullah, M., Naaz, S. F., Iqbal, K. & Lamba, H. S. (2011). *Int. J. Res. Pharm. Chem.* **1**, 565–574.

supporting information

Acta Cryst. (2019). E**75**, 1940-1946 [https://doi.org/10.1107/S2056989019015779]

Crystal structure, Hirshfeld surface analysis and interaction energy and DFT studies of 1-methyl-3-(prop-2-yn-1-yl)-2,3-dihydro-1*H*-1,3-benzodiazol-2-one

Asmaa Saber, Mohamed Srhir, Tuncer Hökelek, Joel T. Mague, Noureddine Hamou Ahabchane, Nada Kheira Sebbar and El Mokhtar Essassi

Computing details

Data collection: *APEX3* (Bruker, 2016); cell refinement: *SAINT* (Bruker, 2016); data reduction: *SAINT* (Bruker, 2016); program(s) used to solve structure: *SHELXT* (Sheldrick, 2015*a*); program(s) used to refine structure: *SHELXL2018* (Sheldrick, 2015*b*); molecular graphics: *DIAMOND* (Brandenburg & Putz, 2012); software used to prepare material for publication: *SHELXTL* (Sheldrick, 2008).

1-Methyl-3-(prop-2-yn-1-yl)-2,3-dihydro-1*H*-1,3-benzodiazol-2-one

Crystal data

$C_{11}H_{10}N_2O$
M_r = 186.21
Monoclinic, $P2_1/n$
a = 7.1507 (3) Å
b = 8.8177 (4) Å
c = 15.4602 (7) Å
β = 97.914 (2)°
V = 965.52 (7) Å^3
Z = 4
$F(000)$ = 392
D_x = 1.281 Mg m^{-3}
Cu $K\alpha$ radiation, λ = 1.54178 Å
Cell parameters from 5848 reflections
θ = 5.8–70.1°
μ = 0.68 mm^{-1}
T = 150 K
Plate, colourless
0.32 × 0.31 × 0.12 mm

Data collection

Bruker D8 VENTURE PHOTON 100 CMOS diffractometer
Radiation source: INCOATEC IμS micro-focus source
Mirror monochromator
Detector resolution: 10.4167 pixels mm^{-1}
ω scans
Absorption correction: multi-scan (*SADABS*; Krause *et al.*, 2015)
T_{min} = 0.83, T_{max} = 0.92
6896 measured reflections
1812 independent reflections
1679 reflections with $I > 2\sigma(I)$
R_{int} = 0.030
θ_{max} = 70.1°, θ_{min} = 5.8°
h = −8→8
k = −10→9
l = −18→18

Refinement

Refinement on F^2
Least-squares matrix: full
$R[F^2 > 2\sigma(F^2)]$ = 0.033
$wR(F^2)$ = 0.086
S = 1.06
1812 reflections
168 parameters
0 restraints
Primary atom site location: dual
Secondary atom site location: difference Fourier map
Hydrogen site location: difference Fourier map
All H-atom parameters refined
$w = 1/[\sigma^2(F_o^2) + (0.0402P)^2 + 0.2239P]$ where $P = (F_o^2 + 2F_c^2)/3$
$(\Delta/\sigma)_{max} < 0.001$

$\Delta\rho_{max}$ = 0.18 e Å^{-3}
$\Delta\rho_{min}$ = −0.19 e Å^{-3}

Extinction correction: *SHELXL2018* (Sheldrick, 2015*b*), Fc*=kFc[1+0.001xFc$^{2}\lambda^{3}$/sin(2θ)]$^{-1/4}$
Extinction coefficient: 0.0100 (12)

Special details

Geometry. All esds (except the esd in the dihedral angle between two l.s. planes) are estimated using the full covariance matrix. The cell esds are taken into account individually in the estimation of esds in distances, angles and torsion angles; correlations between esds in cell parameters are only used when they are defined by crystal symmetry. An approximate (isotropic) treatment of cell esds is used for estimating esds involving l.s. planes.

Refinement. Refinement of F^2 against ALL reflections. The weighted R-factor wR and goodness of fit S are based on F^2, conventional R-factors R are based on F, with F set to zero for negative F^2. The threshold expression of $F^2 > 2\text{sigma}(F^2)$ is used only for calculating R-factors(gt) etc. and is not relevant to the choice of reflections for refinement. R-factors based on F^2 are statistically about twice as large as those based on F, and R- factors based on ALL data will be even larger.

Fractional atomic coordinates and isotropic or equivalent isotropic displacement parameters (Å^2)

	x	*y*	*z*	U_{iso}*/U_{eq}
O1	0.31019 (11)	0.82725 (9)	0.64517 (6)	0.0345 (2)
N1	0.24854 (12)	0.64929 (11)	0.53316 (6)	0.0280 (2)
N2	0.36075 (12)	0.56773 (10)	0.66470 (6)	0.0250 (2)
C1	0.33940 (14)	0.44082 (11)	0.61080 (7)	0.0235 (2)
C2	0.37638 (15)	0.28918 (12)	0.62754 (8)	0.0289 (3)
H2	0.426 (2)	0.2543 (16)	0.6872 (10)	0.039 (4)*
C3	0.34025 (16)	0.18941 (14)	0.55731 (8)	0.0353 (3)
H3	0.364 (2)	0.0783 (17)	0.5684 (10)	0.043 (4)*
C4	0.27117 (17)	0.24106 (15)	0.47421 (8)	0.0378 (3)
H4	0.246 (2)	0.1678 (17)	0.4255 (10)	0.046 (4)*
C5	0.23359 (16)	0.39392 (15)	0.45751 (7)	0.0339 (3)
H5	0.190 (2)	0.4305 (16)	0.3992 (10)	0.042 (4)*
C6	0.26803 (14)	0.49324 (12)	0.52720 (7)	0.0255 (3)
C7	0.30715 (14)	0.69684 (12)	0.61712 (7)	0.0260 (2)
C8	0.17860 (17)	0.75002 (16)	0.46162 (8)	0.0381 (3)
H8A	0.255 (3)	0.747 (2)	0.4146 (13)	0.076 (6)*
H8B	0.176 (3)	0.854 (2)	0.4867 (13)	0.072 (5)*
H8C	0.044 (2)	0.7264 (17)	0.4370 (10)	0.047 (4)*
C9	0.44506 (16)	0.56993 (13)	0.75585 (7)	0.0283 (3)
H9A	0.4344 (19)	0.6753 (16)	0.7764 (9)	0.033 (3)*
H9B	0.376 (2)	0.5012 (16)	0.7898 (9)	0.038 (3)*
C10	0.64427 (15)	0.52362 (12)	0.76752 (7)	0.0281 (3)
C11	0.80385 (17)	0.48197 (14)	0.77883 (8)	0.0342 (3)
H11	0.938 (2)	0.4443 (17)	0.7926 (10)	0.050 (4)*

Atomic displacement parameters (Å^2)

	U^{11}	U^{22}	U^{33}	U^{12}	U^{13}	U^{23}
O1	0.0298 (4)	0.0254 (4)	0.0471 (5)	0.0006 (3)	0.0015 (3)	−0.0012 (3)
N1	0.0239 (4)	0.0309 (5)	0.0277 (5)	−0.0020 (3)	−0.0012 (4)	0.0074 (4)
N2	0.0254 (5)	0.0249 (5)	0.0236 (4)	0.0005 (3)	−0.0007 (3)	−0.0007 (3)
C1	0.0196 (5)	0.0264 (5)	0.0244 (5)	−0.0023 (4)	0.0028 (4)	−0.0014 (4)

C2	0.0249 (5)	0.0281 (6)	0.0337 (6)	−0.0008 (4)	0.0041 (4)	0.0011 (4)
C3	0.0298 (6)	0.0300 (6)	0.0469 (7)	−0.0021 (4)	0.0088 (5)	−0.0072 (5)
C4	0.0339 (6)	0.0427 (7)	0.0384 (6)	−0.0083 (5)	0.0107 (5)	−0.0158 (5)
C5	0.0286 (6)	0.0486 (7)	0.0248 (6)	−0.0089 (5)	0.0048 (4)	−0.0032 (5)
C6	0.0207 (5)	0.0307 (6)	0.0254 (5)	−0.0046 (4)	0.0037 (4)	0.0014 (4)
C7	0.0189 (5)	0.0261 (5)	0.0328 (6)	−0.0007 (4)	0.0025 (4)	0.0025 (4)
C8	0.0294 (6)	0.0450 (7)	0.0380 (7)	−0.0013 (5)	−0.0019 (5)	0.0189 (6)
C9	0.0296 (6)	0.0332 (6)	0.0218 (5)	0.0004 (4)	0.0019 (4)	−0.0014 (4)
C10	0.0333 (6)	0.0293 (5)	0.0206 (5)	−0.0018 (4)	−0.0004 (4)	0.0014 (4)
C11	0.0330 (6)	0.0381 (6)	0.0298 (6)	0.0022 (5)	−0.0016 (4)	0.0030 (5)

Geometric parameters (Å, º)

O1—C7	1.2281 (13)	C4—C5	1.3915 (19)
N1—C7	1.3735 (14)	C4—H4	0.989 (16)
N1—C6	1.3874 (15)	C5—C6	1.3839 (16)
N1—C8	1.4526 (14)	C5—H5	0.967 (15)
N2—C7	1.3807 (14)	C8—H8A	0.97 (2)
N2—C1	1.3910 (13)	C8—H8B	0.99 (2)
N2—C9	1.4545 (14)	C8—H8C	1.004 (16)
C1—C2	1.3805 (15)	C9—C10	1.4689 (16)
C1—C6	1.4011 (14)	C9—H9A	0.988 (14)
C2—C3	1.3937 (17)	C9—H9B	0.978 (15)
C2—H2	0.991 (15)	C10—C11	1.1885 (17)
C3—C4	1.3883 (19)	C11—H11	1.009 (16)
C3—H3	1.005 (15)		
O1···H9A	2.491 (14)	C11···O1^{vii}	3.1569 (15)
O1···H3^{i}	2.566 (15)	C2···H8A^{iv}	2.82 (2)
O1···H8B	2.516 (19)	C3···H8C^{v}	2.859 (15)
O1···H9B^{ii}	2.346 (14)	C3···H8A^{iv}	2.92 (2)
O1···H11^{iii}	2.181 (15)	C4···H8C^{v}	2.810 (15)
C2···C10	3.3889 (16)	C5···H8C^{v}	2.935 (15)
C3···C8^{iv}	3.5335 (17)	C8···H5	2.983 (14)
C4···C8^{v}	3.4947 (17)	C9···H2	2.975 (14)
C4···C7^{iv}	3.5437 (16)	C10···H4^{viii}	2.976 (15)
C5···C8^{v}	3.5884 (17)	C11···H5^{iv}	2.865 (15)
C6···C6^{iv}	3.5349 (14)	C11···H4^{viii}	2.705 (15)
C9···O1^{vi}	3.3198 (14)		
C7—N1—C6	110.19 (9)	C5—C6—N1	132.12 (10)
C7—N1—C8	124.14 (10)	C5—C6—C1	120.83 (11)
C6—N1—C8	125.66 (10)	N1—C6—C1	107.04 (9)
C7—N2—C1	110.16 (9)	O1—C7—N1	127.43 (10)
C7—N2—C9	123.55 (9)	O1—C7—N2	126.43 (10)
C1—N2—C9	126.00 (9)	N1—C7—N2	106.14 (9)
C2—C1—N2	131.64 (10)	N1—C8—H8A	112.7 (12)
C2—C1—C6	121.90 (10)	N1—C8—H8B	106.7 (11)

N2—C1—C6	106.45 (9)	H8A—C8—H8B	111.1 (16)
C1—C2—C3	117.07 (11)	N1—C8—H8C	111.9 (9)
C1—C2—H2	120.7 (8)	H8A—C8—H8C	108.5 (15)
C3—C2—H2	122.3 (8)	H8B—C8—H8C	105.7 (13)
C4—C3—C2	121.20 (11)	N2—C9—C10	112.38 (9)
C4—C3—H3	120.5 (9)	N2—C9—H9A	106.5 (8)
C2—C3—H3	118.3 (9)	C10—C9—H9A	109.8 (8)
C3—C4—C5	121.63 (11)	N2—C9—H9B	109.9 (8)
C3—C4—H4	119.6 (9)	C10—C9—H9B	108.2 (8)
C5—C4—H4	118.8 (9)	H9A—C9—H9B	110.1 (11)
C6—C5—C4	117.35 (11)	C11—C10—C9	177.63 (12)
C6—C5—H5	120.9 (8)	C10—C11—H11	176.1 (9)
C4—C5—H5	121.7 (8)		

C7—N2—C1—C2	178.91 (11)	C2—C1—C6—C5	−0.69 (15)
C9—N2—C1—C2	4.89 (17)	N2—C1—C6—C5	178.96 (9)
C7—N2—C1—C6	−0.69 (11)	C2—C1—C6—N1	−179.67 (9)
C9—N2—C1—C6	−174.72 (9)	N2—C1—C6—N1	−0.02 (11)
N2—C1—C2—C3	−179.33 (10)	C6—N1—C7—O1	179.51 (10)
C6—C1—C2—C3	0.23 (15)	C8—N1—C7—O1	0.13 (17)
C1—C2—C3—C4	0.37 (16)	C6—N1—C7—N2	−1.13 (11)
C2—C3—C4—C5	−0.54 (18)	C8—N1—C7—N2	179.49 (9)
C3—C4—C5—C6	0.08 (17)	C1—N2—C7—O1	−179.51 (10)
C4—C5—C6—N1	179.20 (11)	C9—N2—C7—O1	−5.31 (16)
C4—C5—C6—C1	0.52 (15)	C1—N2—C7—N1	1.12 (11)
C7—N1—C6—C5	−178.10 (11)	C9—N2—C7—N1	175.32 (9)
C8—N1—C6—C5	1.27 (18)	C7—N2—C9—C10	−111.11 (11)
C7—N1—C6—C1	0.72 (11)	C1—N2—C9—C10	62.16 (13)
C8—N1—C6—C1	−179.91 (9)		

Symmetry codes: (i) *x*, *y*+1, *z*; (ii) −*x*+1/2, *y*+1/2, −*z*+3/2; (iii) −*x*+3/2, *y*+1/2, −*z*+3/2; (iv) −*x*+1, −*y*+1, −*z*+1; (v) −*x*, −*y*+1, −*z*+1; (vi) −*x*+1/2, *y*−1/2, −*z*+3/2; (vii) −*x*+3/2, *y*−1/2, −*z*+3/2; (viii) *x*+1/2, −*y*+1/2, *z*+1/2.

Hydrogen-bond geometry (Å, º)

*Cg*1 is the centroid of the C1–C6 benzene ring.

D—H···*A*	*D*—H	H···*A*	*D*···*A*	*D*—H···*A*
C3—H3···O1^{ix}	1.005 (15)	2.566 (15)	3.4885 (15)	152.6 (11)
C8—H8*C*···*Cg*1^{v}	1.004 (16)	2.626 (15)	3.5413 (13)	151.1 (12)
C9—H9*B*···O1^{vi}	0.978 (15)	2.347 (15)	3.3198 (14)	172.9 (12)
C11—H11···O1^{vii}	1.010 (15)	2.181 (15)	3.1569 (15)	162.1 (12)

Symmetry codes: (v) −*x*, −*y*+1, −*z*+1; (vi) −*x*+1/2, *y*−1/2, −*z*+3/2; (vii) −*x*+3/2, *y*−1/2, −*z*+3/2; (ix) *x*, *y*−1, *z*.